J Mater Sci (2013) 48:5607–5613
DOI 10.1007/s10853-013-7355-0

Structural and piezoelectric properties of barium-modified lead-free $(K_{0.455}Li_{0.045}Na_{0.5})(Nb_{0.9}Ta_{0.1})O_3$ ceramics

Roopam Gaur · K. Chandramani Singh · Radhapiyari Laishram

Received: 14 December 2012 / Accepted: 28 March 2013 / Published online: 9 April 2013

Abstract Ferroelectric $(K_{0.455}Li_{0.045}Na_{0.5})(Nb_{0.9}Ta_{0.1})O_3$ + x mol% $BaCO_3$ ceramic compositions with Ba^{2+} as an A-site dopant in the range of $x = 0$–1.2 mol% were synthesized by conventional ceramic processing route. Effect of Ba^{2+} content on the microstructure, ferroelectric, dielectric, and piezoelectric properties of the ceramics was investigated. The results of X-ray diffraction reveal that Ba^{2+} diffuse into the $(K_{0.455}Li_{0.045}Na_{0.5})(Nb_{0.9}Ta_{0.1})O_3$ lattices to form a solid solution with a perovskite structure having typical orthorhombic symmetry. As Ba^{2+} content increases, cell volume and tetragonality increase in the crystal structure of the ceramics. Increasing doping level of Ba^{2+} inhibits grain growth in the ceramics and reduces both the Curie temperature (T_c) and tetragonal–orthorhombic phase transition temperature ($T_{o\text{-}t}$). The bulk density, remnant polarization P_r, room-temperature dielectric constant (ε'_{RT}), planar electromechanical coupling factor k_p, and piezoelectric charge coefficient d_{33} are found to increase as Ba^{2+} concentration increases from 0 to 0.8 mol% and then decrease as Ba^{2+} content increases further from 0.8 to 1.2 mol%. High piezoelectric properties of $d_{33} = 187$ pC/N and $k_p = 48$ % are found in 0.8 mol% Ba^{2+} composition. Optimum amount of Ba^{2+} dopant takes the polymorphic phase boundary region consisting of orthorhombic and tetragonal crystal structures of the ceramic system near the room temperature and enhances its piezoelectric properties.

R. Gaur · K. C. Singh (✉)
Department of Physics, Sri Venkateswara College, University of Delhi, New Delhi 110021, India
e-mail: kongbam@gmail.com

R. Laishram
Solid State Physics Laboratory, Lucknow Road, Timarpur, Delhi 110054, India

Introduction

Lead-based perovskite ceramics, such as PZT, have been extensively used in actuators, sensors, and transducers due to their excellent electrical, piezoelectric, and electromechanical properties [1, 2]. However, their high content of a toxic element (Pb > 60 wt%) has caused serious environmental and safety concerns. As a result, there have been considerable efforts made in recent years to find alternative lead-free piezoelectric ceramics with properties comparable to their lead-based counterparts [3, 4]. Among the lead-free piezoelectric alternatives, potassium sodium niobate (K,Na)NbO_3 solid solution, with the composition $(K_{0.5}Na_{0.5})NbO_3$ (KNN) being close to the morphotropic phase boundary, is one of the most promising candidates because of its good piezoelectric properties and high Curie temperature (T_c) [5, 6]. Pure KNN ceramics are however difficult to sinter under ordinary conditions and exhibit relatively poor piezoelectric properties [7].

Sintering aids [8, 9], spark plasma sintering [10], templated grain growth [7], and hot pressing [11] have been used to obtain high densities in KNN ceramics. Though these processes yield high density and better piezoelectric properties than conventional sintering of KNN, they still require careful processing parameters compared to the conventional air-sintering process. Therefore, these techniques are not always appropriate for industrial use in terms of process cost and mass productivity. Modification in the composition of KNN ceramics is therefore desirable to enhance densification and in turn piezoelectric properties. KNN ceramics substituted suitably with elements like Li, Ta, and Sb, have yielded enhanced piezoelectric and electromechanical properties [5, 7, 12–15]. Among the Li- and Ta-modified KNN ceramics, optimum piezoelectric properties have been obtained in several compositions,

such as, $(K_{0.5}Na_{0.5})_{0.96}Li_{0.04}(Nb_{0.90}Ta_{0.10})O_3$ [7], and $(K_{0.5}Na_{0.5})_{0.96}Li_{0.04}(Nb_{0.775}Ta_{0.225})O_3$ [16]. The ceramic composition $K_{0.455}Na_{0.5}Li_{0.045}(Nb_{0.90}Ta_{0.10})O_3$ has been reported [17] to show reasonably high density with the orthorhombic–tetragonal transition temperature ($T_{o\text{-}t}$) occurring at 88 °C, which is conveniently closer to room temperature compared with 190 °C observed for KNN [18].

In Ba-doped PLZT system, it has been found that [19] with increasing Ba^{2+}concentration grain growth is inhibited, room-temperature dielectric constant and piezoelectric properties increase from the composition with no Ba^{2+} to that with 4 % Ba^{2+}.

In the present study we investigate the effect of Ba^{2+} as donor-dopant on the ferroelectric and piezoelectric properties of the $(K_{0.455}Na_{0.5}Li_{0.045})(Nb_{0.9}Ta_{0.1})O_3$ (KNLNT) system. The choice of Ba^{2+} as an A-site substituent is made on the basis of its compatible ionic size and coordination number. This study is of special importance compared with other similar substitution works reported in KNN system, as it takes advantage of two features which could create a PPT near the room temperature and hence enhance the piezoelectric properties of the system. First is the selection of Ba^{2+} substituent which possesses the possibility of reducing $T_{o\text{-}t}$ in the KNN system and second is the choice of KNLNT as the base system for which $T_{o\text{-}t}$ occurs at a low value of 88 °C.

Experimental

$(K_{0.455}Na_{0.5}Li_{0.045})(Nb_{0.9}Ta_{0.1})O_3$ powders were synthesized through the conventional mixed oxide route from the following analytical-grade raw materials: K_2CO_3, Na_2CO_3, Li_2CO_3, Nb_2O_5, and Ta_2O_5 (≥99.99 %, Aldrich), which were dried at 200 °C before use. The powders were homogeneously mixed in a plastic bottle using ball milling with isopropyl alcohol as solvent and 2-mm zirconia balls as milling media. They were then calcined at 900 °C for 4 h in air. To obtain compositional homogeneity in the mixture, the ball milling and calcination were repeated. The preparation of compositions $(K_{0.455}Na_{0.5}Li_{0.045})_{1\text{-}2x}Ba_x(Nb_{0.9}Ta_{0.1})O_3$ with various ($x = 0$, 0.4, 0.8, 1.0, and 1.2) mol% of Ba^{2+} was performed by milling the appropriate molar ratio of calcined powders and $BaCO_3$ in isopropyl alcohol medium, using a Retsch PM 100 planetary ball mill with Agate vial and balls. The milling was performed at the speed of 300 rpm for 1 h with the rotational direction of the vial and the sun wheel reversing every 6 min after a rest interval of 2 min. A mass ratio of 1:5 for powder and balls was always maintained during milling.

After drying, the milled powders were granulated by adding 5-wt% poly vinyl alcohol as a binder and were uniaxially pressed into circular pellets of 10 mm diameter and 1 mm thickness at 200 MPa. After burning off the binder, the pellets were sintered in a covered alumina crucible at 1050 °C for 2 h in air. The sintered pellets were lapped to a thickness of 0.6 mm. These sintered ceramic samples corresponding to $x = 0$, 0.4, 0.8, 1.0, and 1.2 will be referred as KNLNTB0, KNLNTB4, KNLNTB8, KNLNTB10, and KNLNTB12, respectively.

The bulk density of the sintered compacts was obtained by Archimedes method. X-ray Diffractometer (Philips Diffractometer PW 3020) with monochromatic CuK_α radiation ($\lambda = 1.54178$Å) was used over a 2θ angle from 20° to 70° to determine the crystal structures of the sintered specimens. The microstructures of the fractured surfaces of the samples were studied using SEM (Leo 1430, Japan). Average grain size measurements of the sintered ceramics were carried out using the mean intercept length method from at least five different areas of sample. For electrical measurements, silver paste was applied on both sides of the sintered samples as electrodes and fired at 200 °C for 1 h. The ferroelectric hysteresis loops of the ceramics were measured at room temperature using an automated *P–E* loop tracer (AR Imagetronics, India) operating at 50 Hz. The temperature dependence of dielectric properties was measured with an impedance analyzer (Wayne Kerr 6505B). For activating piezoelectric properties to the ceramics, the samples were immersed in silicone oil and poled under a DC field of 3 kV/mm at 100 °C for 30 min, and then the samples were cooled to room temperature by maintaining the electric field. The electromechanical coupling factor (k_p) has been calculated from the resonance–antiresonance frequencies recorded by the impedance analyzer. The piezoelectric charge coefficient (d_{33}) was measured with a Piezometer (Take Control, PM 25).

Results and discussion

Figure 1a shows the XRD patterns of the sintered ceramics with different molar percentages of Ba^{2+}. It is found that all the ceramic samples crystallize into a pure perovskite structure with no secondary phase. This suggests that Ba^{2+} has diffused into the $(K_{0.455}\ Na_{0.5}Li_{0.045})(Nb_{0.9}Ta_{0.1})O_3$ lattices to form a homogeneous solid solution. All perovskite peaks in the XRD patterns can be attributed to the $KNbO_3$ structure with JCPDS No. 71-0946 in the ICDD database, $KNbO_3$ being taken as a reference because it is iso-structural with KNN. The crystal structure possesses orthorhombic symmetry specified by the splitting of the (022) and (200) reflections and higher intensity counts for the (022) peaks shown clearly in the enlarged diagram of Fig. 1a. The values of the lattice parameters calculated for various ceramic samples are summarized in Table 1.

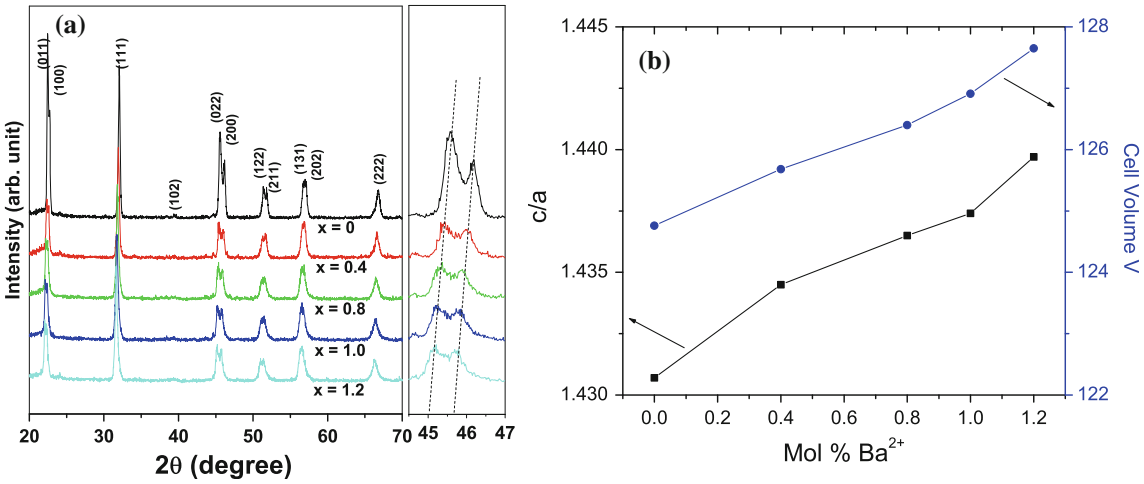

Fig. 1 **a** XRD patterns, and **b** *c/a* ratio and unit cell volume, of KNLNTB ceramics with $x = 0$, 0.4, 0.8, 1.0, and 1.2 mol% Ba^{2+}

Table 1 Several properties of $(K_{0.455}\ Na_{0.5}Li_{0.045})(Nb_{0.9}Ta_{0.1})O_3 + x$ mol% $BaCO_3$ ceramics

Parameter	$x = 0$	$x = 0.4$	$x = 0.8$	$x = 1.0$	$x = 1.2$
Lattice constants (Å)					
a	3.9339	3.9458	3.9506	3.9575	3.9652
b	5.6306	5.6272	5.6376	5.6452	5.6392
c	5.6281	5.6601	5.6750	5.6887	5.7088
P_r (μC/cm^2)	8.4	10.6	15.4	7.8	4.9
E_c (kV/cm)	3.9	5.8	6.7	5.4	4.6
ε'_{RT} (100 kHz, 25 °C)	553	573	590	515	481
T_c	451	448	443	429	404
$T_{o\text{-}t}$	88	60	48	–	–
k_p(%)	38	43	48	37	31
d_{33}(pC/N)	123 ± 2	145 ± 3	187 ± 3	121 ± 2	92 ± 2

With increasing Ba^{2+} doping, there is a gradual shift of the diffraction peaks toward lower angle indicating an increase in the lattice cell volume. The dependence of cell volume determined for all the ceramic samples on Ba^{2+} content is explicitly shown in Fig. 1b. The gradual enlargement of cell volume in this figure suggests that Ba^{2+} ions (ionic radii ≈ 1.36Å) are possibly incorporated into the perovskite structure. On ionic size and coordination number considerations, the cation lattice sites, such as those of K^+ (ionic radii ≈ 1.38Å) or Na^+ ions (ionic radii ≈ 1.02Å) are locations with the highest possibility of occupation by Ba^{2+} ions. Due to close proximity of the ionic radii, Ba^{2+} ions replacing K^+ may be more probable. However, the observed gradual increase in cell volume with increasing Ba^{2+} content indicates that Na^+ ions are also getting proportionately substituted by Ba^{2+} ions in the present composition range.

Figure 1b also shows the variation of tetragonality (*c/a*) in the ceramics with Ba^{2+} content. The slight increase in tetragonality as shown in Fig. 1b is suggestive of a lowering of $T_{o\text{-}t}$ toward the room temperature, consequent upon increasing Ba^{2+} doping in the KNLNTB system. Such a lowering of $T_{o\text{-}t}$ with increasing Ba^{2+} content has also been observed in KNN system [20].

There are mixed reports [21, 22] of modification in the crystal structure of pure KNN system when doped with Ba. In $(Ba_xK_{0.5-x}Na_{0.5-x})NbO_3$ system, the crystal structures are reported to change from orthorhombic to pseudocubic with Ba content above $x = 0.03$ [21]. In $(K_{0.5}Na_{0.5})_{1-2y}Ba_yNbO_3$ system, even a low amount of Ba-doping (0.5 mol%) leads to the appearance of a secondary phase [22]. However, in the present study, even for 1.2 mol% Ba^{2+} content, the KNLNTB system remains in the orthorhombic phase with no secondary phase. This possibility can be attributed to the lower $T_{o\text{-}t}$ of our base KNLNT ceramics (88 °C) compared with that of pure KNN ceramics (190 °C). As $T_{o\text{-}t}$ further decreases with increasing Ba^{2+} content, more and more of tetragonal structures are built up in the ceramic system near the room temperature. Existence of two structurally different crystalline phases—orthorhombic and tetragonal—simultaneously in the system may result in the increase of overall solubility of Ba^{2+} in the system. The important role of crystal structure of the host on the solution energy and in turn the solid solubility in transition metal alloys has been discussed [23]. Moreover, the unspecified mode of A-site Ba-doping used in the present study unlike the constrained ones reported earlier [21, 22] also facilitates the higher intake of Ba^{2+} by the ceramic system without forming any secondary phase.

The internal strain η values of the ceramics were calculated using the following equation [24]:

$$\beta \cos\theta = \frac{\lambda}{d} + 2\eta \sin\theta$$

where β is the full-width at half-maximum (FWHM) of the X-ray diffraction peaks, λ is the wavelength of X-rays

(CuK_α: $\lambda = 1.54178$Å), and d is the size of the crystallite. Since d is sufficiently larger than λ, the above equation can be simplified as:

$$\beta = 2\eta \tan\theta$$

The internal strains $\eta_{(011)}$ and $\eta_{(100)}$ calculated for various values of Ba^{2+} contents in the ceramics are plotted in Fig. 2. As seen in this figure, the internal strain $\eta_{(011)}$ increases from 5.2×10^{-3} to the maximum value of 6.9×10^{-3} in the x range from 0.8 to 1.0, then decreases to 5.2×10^{-3} at $x = 1.2$. On the other hand, the internal strain $\eta_{(100)}$ increases from 6.1×10^{-3} to the maximum value of 6.9×10^{-3} in the x range from 0 to 0.4 and then decreases to 5.2×10^{-3} at $x = 0.8$. These observations suggest that the structural transformation of the crystal produced by increasing Ba^{2+} content in KNLNTB cell initiate around the (011) plane, and then spread to the (100) plane of orthorhombic perovskite structure with space group *Bmm2*, as the crystal structure gradually transforms into tetragonal perovskite structure with space group *P4 mm*. The changeover in the variations of $\eta_{(011)}$ and $\eta_{(100)}$ with Ba^{2+} content observed at $x = 0.8$ indicates that a large anisotropic strain exists in the crystal lattice around the 0.8 mol% Ba^{2+} composition.

Figure 3 shows the microstructures of the fractured surfaces of the as-sintered ceramics. Abnormal grain growth is observed in the microstructure of these ceramics, which consisted of both large and small grains. The grains are facetted with clear-cut edges and plane faces at right angles to each other, which are typical characteristics of KNN system. It can be noted from Fig. 3c that the KNLNTB8 sample is relatively more densely-packed and has a homogeneous microstructure with a uniform grain size.

Figure 4 shows the effect of Ba^{2+} content on the bulk density and average grain size of the ceramics. As Ba^{2+} concentration increases, the bulk density gradually

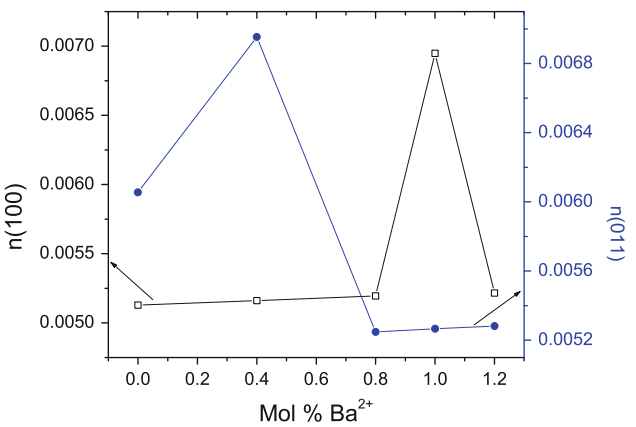

Fig. 2 Internal strains $\eta_{(011)}$ and $\eta_{(100)}$ for various values of Ba^{2+} contents in KNLNTB ceramics

increases from 4.12 g/cm^3 for the ceramic composition with no Ba^{2+} to the maximum value of 4.63 g/cm^3 for 0.8 mol% Ba^{2+} and then decreases to 3.97 g/cm^2 for 1.2 mol% Ba^{2+}. The grains have an average diameter in the range of about 0.8–5.2 μm. The average grain size shows a decreasing trend with increasing Ba^{2+} content. This indicates that Ba^{2+} addition effectively inhibits the grain growth in KNLNT system. This observation is in agreement with the effect of Ba^{2+} addition in KNN system [20]. Ba^{2+} concentrates near the grain boundaries restricting their mobility as densification occurs. The reduction in the mobility of the grain boundary weakens the mass transportation and results in grain growth inhibition with increasing Ba^{2+} content [25]. The KNLNTB8 sample has the highest density having intermediate average grain size of about 3 μm. With increasing Ba^{2+} content, the grains further decrease in size and for KNLNTB12 sample the grains are extremely fine, less than 1 μm.

The increase in density for ceramics in the range of 0–0.8 mol% Ba^{2+} contents is in agreement with the observed increasing homogeneity in grains. A-site substitution by Ba^{2+} ions creates A-site atomic vacancies in the perovskite structure to maintain charge balance in the lattice, which also provides a basis for the enhanced sinterability in the ceramics. The decline in density of the ceramics observed for Ba^{2+} content more than 0.8 mol% perhaps indicates the existence of a critical grain size (around 3 μm) below which the densification process in the ceramics get weakened. The weakening trend of densification in this composition range can be attributed to the inhomogeneous grain size reduction and trapping of porosity in the microstructure.

Figure 5 shows the polarization–electric field (P–E) hysteresis loops for the KNLNTB ceramics with different molar concentrations of Ba^{2+}, measured at 25 °C and 50 Hz. A well-saturated hysteresis loop was obtained for the composition KNLNTB0. Increase of the Ba^{2+} concentration gave rise to unsaturated hysteresis loops. From the P–E hysteresis loops in Fig. 5, P_r and E_c were determined for the ceramics and are presented in Table 1. For the base composition KNLNTB0, the remnant polarization P_r is 8.4 μC/cm^2 and the coercive field E_c is 3.9 kV/cm. With increasing Ba^{2+} content, P_r increases, reaches a maximum value of ~15.4 μC/cm^2 at 0.8 mol% Ba^{2+} content and then decreases to 4.9 μC/cm^2 at 1.2 mol% Ba^{2+} content. The monotonous increase in the P_r value in the range 0–0.8 mol% Ba^{2+} content shows that ferroelectricity of KNLNTB improves with increasing Ba^{2+} content in this range.

The observed decrease in P_r at higher Ba^{2+} concentrations of 1.0 and 1.2 mol% may be attributed to the effect of Ba^{2+} on reducing the grain size which in turn results in a decrease in domain size. Arlt et al. [26] also have shown in $BaTiO_3$ that the equilibrium domain width is dependent on

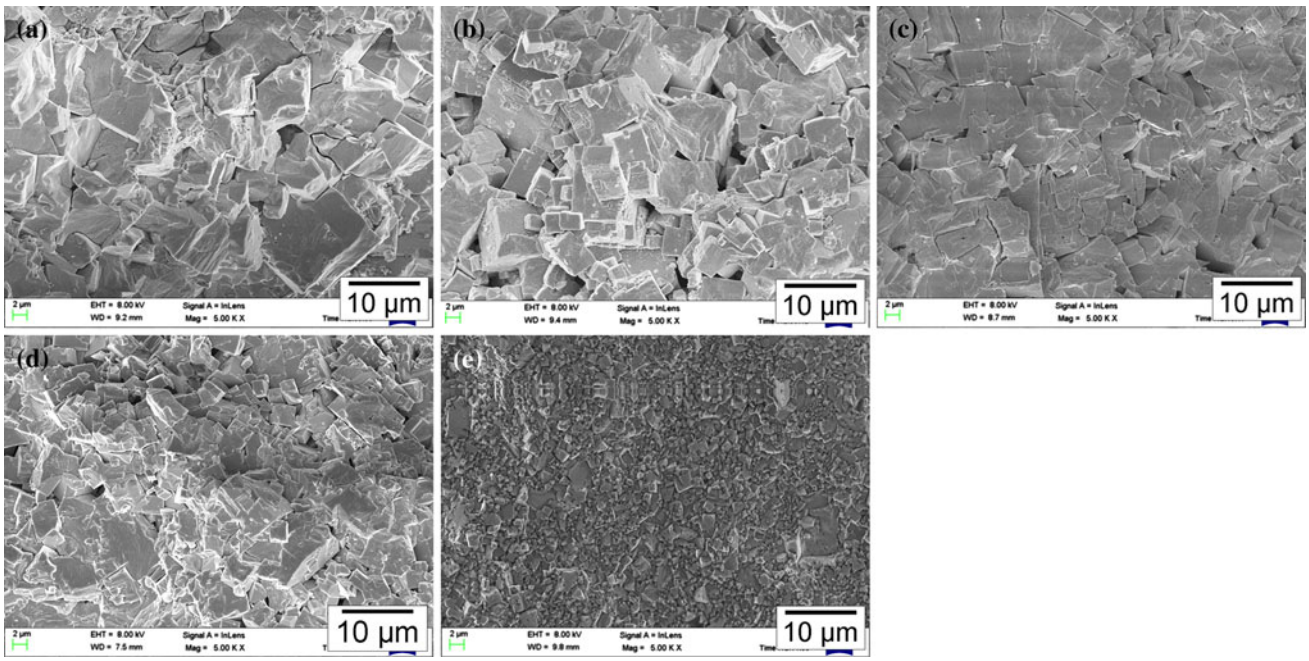

Fig. 3 SEM micrographs of KNNLT ceramics modified with Ba^{2+} concentrations of **a** 0 mol%, **b** 0.4 mol%, **c** 0.8 mol%, **d** 1.0 mol%, and **e** 1.2 mol%

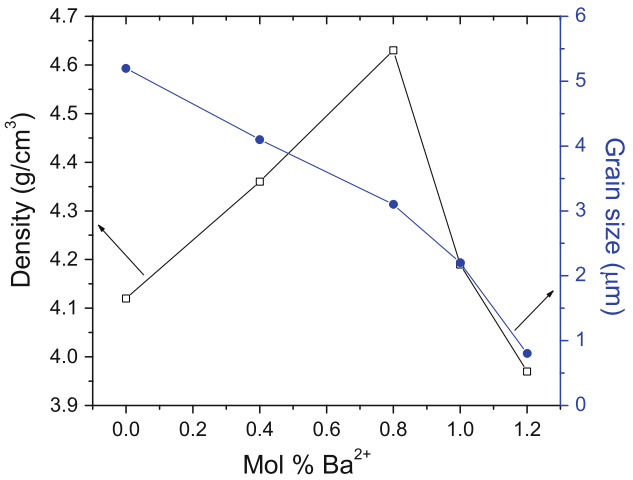

Fig. 4 Plots of bulk density and average grain size of KNLNTB ceramics against Ba^{2+} content

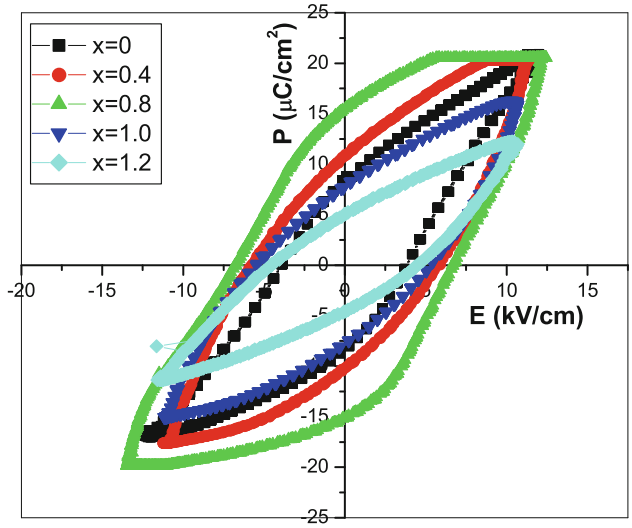

Fig. 5 *P–E* hysteresis curves for KNLNTB ceramics with $x = 0$, 0.4, 0.8, 1.0, and 1.2 mol% Ba^{2+}, measured at 25 °C and 50 Hz

the grain size and decreases for grain sizes <10 μm, and is effectively constant at grain size >10 μm. In the present study, significant decrease in P_r is observed when the grain size is smaller than 3.1 μm, which corresponds to Ba^{2+} content greater than 0.8 mol%. The observed decrease in P_r with increasing Ba^{2+} content has also been reported for KNN system [27].

Figure 6 shows the temperature dependence of dielectric constant (ε') for KNLNTB ceramics with different molar concentrations of Ba^{2+}, measured at 100 kHz. In agreement with the previous work [17], the KNLNTB0 ceramic exhibits two transition peaks: one is associated with the cubic–tetragonal phase transition at 451 °C (T_c) and the other is the tetragonal–orthorhombic phase transition at 88 °C ($T_{o\text{-}t}$). After the doping of Ba^{2+} for the A-site ions, the KNLNTB ceramics exhibit similar temperature dependences of ε', but with the two transition peaks shifted to lower temperatures and the widths of the dielectric peaks broadened. In addition, the corresponding highest ε' value of KNLNTB ceramics at T_c decreases with increasing Ba^{2+} content. The broadening of the dielectric peaks with

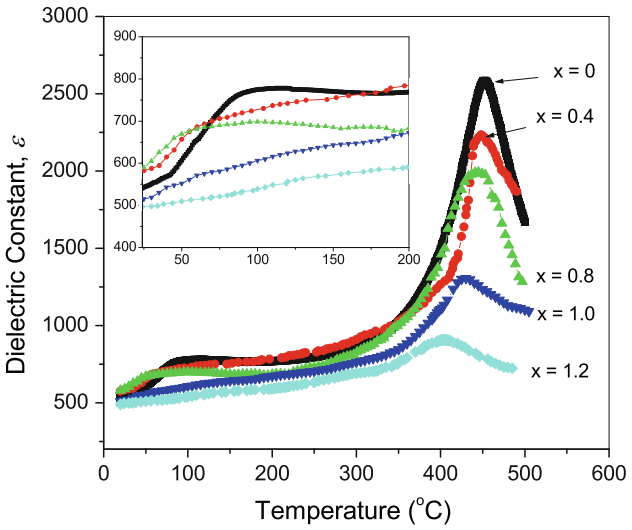

Fig. 6 Temperature dependence of dielectric constant for KNLNTB ceramics with $x = 0$, 0.4, 0.8, 1.0, and 1.2 mol% Ba^{2+}, measured at 100 kHz

increase in Ba^{2+} content can be attributed to the decreasing grain size of the ceramics.

The room-temperature dielectric constant ε'_{RT} of the samples initially increases in accordance with the shift of the transition toward the lower-temperature region and reaches its maximum value of 590 at 0.8 mol%, and it then decreases with further increase of Ba^{2+} content. The dielectric constant ε'_{RT} decline when Ba^{2+} content >0.8 mol% can be attributed to the corresponding fall of density of the sintered samples.

Table 1 shows the values of d_{33} of the ceramics for different molar concentrations of Ba^{2+}. The change observed in d_{33} is in accordance with the change in the density, P_r and ε'_{RT} of the ceramics. When the content of Ba^{2+} is increased, the d_{33} values of the ceramics increase and the highest value ($d_{33} = 187$ pC/N) is recorded at 0.8 mol%. The increase in d_{33} can be attributed to the dominant effect of doping of the soft additive Ba^{2+} ions on the A-sites, rather than that of the hard additive Na^+ and K^+ ions. The shifting of $T_{o\text{-}t}$ in the vicinity of room temperature with increasing Ba^{2+}, as discussed in the XRD and dielectric constant results, could be another contributing factor to the increase in d_{33}. This would result in setting up a polymorphic phase boundary (PPB) between orthorhombic and tetragonal structures which can consequently enhance the piezoelectric property of the ceramics owing to the coexistence of their multiple spontaneous polarization vectors. Contribution to the large d_{33} at 0.8 mol% Ba^{2+} content could also come from the large anisotropic strain existing in the crystal lattice around the 0.8 mol% Ba^{2+} composition, as evident from the XRD result. The presence of such a strain could possibly result in an anisotropic distortion of the NbO_6 octahedral of KNLNTB8 which promotes a preferential Nb off-centre and becomes an origin for the enhancement of their spontaneous polarization and hence piezoelectric properties. In addition, the more homogeneous and dense microstructure of KNLNTB8 ceramics achieved by the addition of Ba^{2+} also plays a vital role in its higher value of d_{33}.

As seen in Table 1, further increase in the doping level of Ba^{2+} in the ceramics from 0.8 mol%, results in a decrease in the d_{33} value. This decrease in d_{33} may be due to a cumulative effect of density decrease and smaller grain size of the ceramics. The small grains of the KNLNTB10 and KNLNTB12 ceramics probably have the effect of suppressing the lattice distortion resulting from the cubic lattice and, hence, lead to the degradation of piezoelectricity. Moreover, with the reduction in grain size, the crystallite size would also correspondingly reduce to such an extent that other mechanisms like pinning of domain walls set into disrupt the further improvement in piezoelectric behavior with decreasing grain size. The observed lower value of d_{33} in KNLNTB10 and KNLNTB12 thus supports the existence of an appropriate grain size, as observed in $BaTiO_3$, for better piezoelectric properties [28]. The piezoelectric properties in donor-doped PZT are also shown to degrade by constraining domain wall motion at grain boundaries [29] thereby indicating the existence of a critical grain size below which the piezoelectric properties appreciably diminish. Piezoelectric properties are also reported to be strongly affected by grain size in Ba^{2+}-doped KNN system [21].

The piezoelectric properties ($d_{33} = 187$ pC/N, $k_p = 48$ %) observed in the present study are appreciably higher than those of the highest values ($d_{33} = 115$ pC/N, $k_p = 37$ %) reported [20] for Ba-modified KNN ceramics or those ($d_{33} = 105$ pC/N, $k_p = 34$ %) reported [16] for the ceramic composition $(K_{0.48}Na_{0.48}Li_{0.04})(Nb_{0.9}Ta_{0.1})O_3$, which is compositionally close to our base composition $(K_{0.455}\ Na_{0.5}Li_{0.045})(Nb_{0.9}Ta_{0.1})O_3$.

Conclusions

With $(K_{0.455}\ Na_{0.5}Li_{0.045})(Nb_{0.9}Ta_{0.1})O_3$ as the base composition, Ba^{2+} in the range of $x = 0$–1.2 mol% has been added as an A-site dopant to yield ceramic samples having pure perovskite structure. The doping of Ba^{2+} in the ceramics lowers both the cubic–tetragonal phase transition temperature (T_c) and the tetragonal–orthorhombic phase transition temperature ($T_{o\text{-}t}$). Increasing Ba^{2+} content inhibits grain growth in the ceramics. The bulk density, remnant polarization P_r, room-temperature dielectric constant ε'_{RT} and piezoelectric charge coefficient d_{33} are found to increase as Ba^{2+} concentration increases from 0 to

0.8 mol% and then decrease as Ba^{2+} content increases further from 0.8 to 1.2 mol%. The optimum values of d_{33} (187 pC/N) and k_p (48 %) are found in 0.8 mol% Ba^{2+} composition. These enhanced piezoelectric properties are attributed to the denser microstructure having optimum grain size, softer (Ba^{2+}) effect, shifting of $T_{o\text{-}t}$ near the room temperature and a large anisotropic strain existing in the crystal lattice of the KNLNTB8 system.

Acknowledgements The authors acknowledge the financial support from the Department of Science and Technology, India, under the Research Project No. SR/S2/CMP-0017/2011.

References

1. Jaffe B, Cook WR, Jaffe H (1971) Piezoelectric ceramics. Academic, New York, p 115
2. Tressler JF, Alkoy S, Newnham RE (1998) J Electroceram 2:257
3. Gomah-Pettry J-R, Said S, Marchet P, Mercurio J-P (2004) J Eur Ceram Soc 4:1165
4. Liu W, Ren X (2009) Phys Rev Lett 103:257602
5. Hollenstein E, Davis M, Damjanovic D, Setter N (2005) Appl Phys Lett 87:182905
6. Ichiki M, Zhang L, Tanaka M, Maeda R (2004) J Eur Ceram Soc 24:1693
7. Saito Y, Takao H, Tani T, Nonoyama T, Takatori K, Homma T, Nagaya T, Nakamura M (2004) Nature 432:84
8. Matsubara M, Yamaguchi T, Sakamoto W, Kikuta K, Yogo T, Hirano S (2005) J Am Ceram Soc 88:1190
9. Matsubara M, Kikuta K, Hirano S (2005) J Appl Phys 97:114105
10. Li JF, Wang K, Zhang BP, Zhang LM (2006) J Am Ceram Soc 89:706
11. Jaeger RE, Egerton L (1962) J Am Ceram Soc 45:209
12. Guo Y, Kakimoto K, Ohsato H (2004) Appl Phys Lett 85:4121
13. Saito Y, Takao H (2006) Ferroelectrics 338:17
14. Zhang SJ, Xia R, Shrout TR, Zang GZ, Wang JF (2006) J Appl Phys 100:104108
15. Yang ZP, Chang YF, Wei LL (2007) Appl Phys Lett 90:042911
16. Lin D, Kwok KW, Chan HLW (2007) J Appl Phys 102:034102
17. Chandramani Singh K, Chongtham Jiten, Radhapiyari Laishram, Thakur OP, Bhattacharya DK (2010) J Alloy Compd 496:717
18. Tennery VJ, Hang KW (1968) J Appl Phys 39:4749
19. Koduri R, Hermosilla LS (2006) Physica Status Solidi (A) Appl Res 203:2119
20. Ahn ZS, Schulze WA (1987) J Am Ceram Soc 70:C18
21. Tashiro S, Ishii K (2006) J Ceram Soc Jpn 114:386
22. Malic B, Bernard J, Holc J, Jenko D, Kosec M (2005) J Eur Ceram Soc 25:2707
23. Ruban AV, Skriver HL, Norskov JK (1998) Phys Rev Lett 80:1240
24. Stokes AR, Wilson AJC (1944) Proc Phys Soc 56:174
25. Lin D, Kwok KW, Chan HLW (2007) J Phys D Appl Phys 40:6778
26. Arlt G, Hennings D, de With G (1985) J Appl Phys 58:1619
27. Cho JH, Lee YH, Kim BI (2010) J Ceram Proc Res 11:237
28. Takahashi H, Numamoto Y, Tani J, Matsuta K, Qiu J, Tsurekawa S (2006) Jpn J Appl Phys 45:L30
29. Randall CA, Kim N, Kucera J-P, Cao W, Shrout TR (1988) J Am Ceram Soc 81:677